ISTITUTO NAZIONALE DI RICERCA METROLOGICA
Repository Istituzionale

Development and Testing of a System for Controlled Ultrasound Hyperthermia Treatment With a Phantom Device

(Article begins on next page)

30 April 2024

Development and Testing of a System for Controlled Ultrasound Hyperthermia Treatment With a Phantom Device

Aoife M. Ivory, *Member, IEEE*, Raphaela de Melo Baesso, Giovanni Durando,
Srinath Rajagopal, *Member, IEEE*, and Piero Miloro

Abstract—Hyperthermia is the process of raising tissue temperatures in the range 40 °C–45 °C for a prolonged time (up to hours). Unlike in ablation therapy, raising the temperature to such levels does not cause necrosis of the tissue but has been postulated to sensitize the tissue for radiotherapy. The ability to maintain a certain temperature in a target region is key to a hyperthermia delivery system. The aim of this work was to design and characterize a heat delivery system for ultrasound hyperthermia able to generate a uniform power deposition pattern in the target region with a closed-loop control, which would maintain the defined temperature over a defined period. The hyperthermia delivery system presented herein is a flexible design with the ability to strictly control the induced temperature rise with a feedback loop. The system can be reproduced elsewhere with relative ease and is adaptable for various tumor sizes/locations and for other temperature elevation applications, such as ablation therapy. The system was fully characterized and tested on a newly designed custom-built phantom with controlled acoustic and thermal properties and containing embedded thermocouples. Additionally, a layer of thermochromic material was fixed above the thermocouples, and the recorded temperature increase was compared to the red, green, and blue (RGB) color change in the material. The transducer characterization allowed for input voltage to output power curves to be generated, thus allowing for the comparison of power deposition to temperature increase in the phantom. Additionally, the transducer characterization generated a field map of the symmetric field. The system was capable of increasing the temperature of the target area by 6 °C above body temperature and maintains the temperature to within ±0.5 °C over a defined period. The increase in temperature correlated with the RGB image analysis of the thermochromic material. The results of this work have the potential to contribute toward increasing confidence in the delivery of hyperthermia treatment to superficial tumors. The developed system could potentially be used for phantom or small animal proof-of-principle studies. The developed phantom test device may be used for testing other hyperthermia systems.

Index Terms—high intensity focused ultrasound (HIFU), hyperthermia, thermochromic tissue mimicking material (TMM), thermocouple.
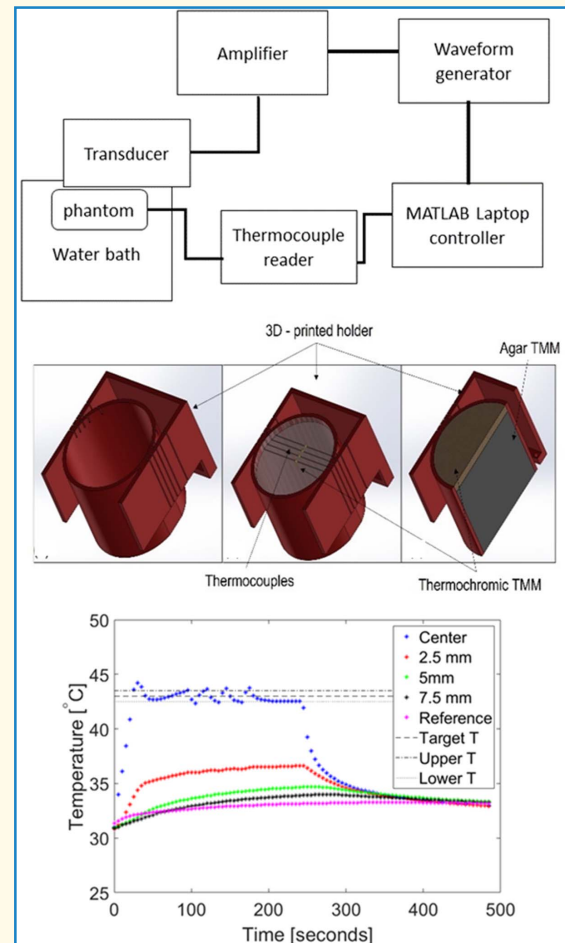
I. INTRODUCTION

HYPERTHERMIA is the process of raising tissue temperatures to abnormally high temperature (40 °C–45 °C). Hyperthermia treatments require the temperature to be kept within this specific range (40 °C–45 °C) for a prolonged time (up to hours) and can be used as a thermal therapy for cancer treatment [1]. Unlike thermal ablation, where temperatures exceeding 60 °C are achieved, hyperthermia does not cause necrosis of the tissue. However, hyperthermia treatment has

Highlights

- **A fully characterized flexible system for hyperthermia delivery and a newly-designed custom-built phantom containing thermochromic material and embedded thermocouples is presented.**

- **The system can increase the temperature of the target area 6 °C above body temperature and maintain the temperature to within ±0.5 °C, the increase in temperature correlated with the RGB image analysis of the thermochromic material.**

- **The results of this work have the potential to contribute towards increasing confidence in the delivery of hyperthermia treatment to superficial tumors.**

long been postulated to sensitize the tissue for both radiotherapy and chemotherapy [2]. Damage to healthy tissue can limit the achievable dose delivered in radiotherapy, but by combining with hyperthermia, the radiosensitivity of the tissue in the target region can be increased by an order of magnitude [3]. Hyperthermia can be used as a technique, which targets increasing oxygenation delivery, increases blood flow, and inhibits DNA repair, providing mechanisms to sensitize tissue to radiotherapy [4] and overcome hypoxia.

The therapeutic effect of hyperthermia treatment combined with radiotherapy treatment depends on several factors, including the time between treatments, the duration of hyperthermia treatment, and the temperature achieved. The combination of the temperature and the duration of heating is known as the thermal dose and is often expressed as the cumulative equivalent minutes at 43 °C (CEM43 °C). CEM43 °C can be used to convert a time-temperature history to an equivalent number of minutes of heating at 43 °C, using the following equation:

$$\mathrm{CEM43°C} = \int t \cdot R^{(T)} \mathrm{d}t \qquad (1)$$

where CEM43 °C is the cumulative number of equivalent minutes at 43 °C, t is time, T is the temperature, and R is related to the temperature dependence of the rate of cell death [$R(T < 43 \text{ °C}) = 1/4$ and $R(T \geq 43 \text{ °C}) = 1/2$].

The resulting CEM43 °C value represents the effect of the entire history of heat exposure [5]. However, it should also be noted that this measure does not account for the effect of sensitization by enhanced oxygenation, variation in interval time, and the effect of multiple hyperthermia fractions [6].

The ability to maintain a certain temperature in a target region is critical to the hyperthermia delivery system. This is important to achieve the desired effects but: 1) ensure that necrosis is not induced (due to increased temperatures consistent with thermal ablation) and 2) ensure healthy tissue is not treated (requiring sufficient localization of the treatment to avoid sensitizing healthy tissue). An accurate knowledge of the temperature change induced, and the thermal dose, also contributes to a better understanding of the therapeutic effects, improves repeatability, and enables multicenter trials, thus facilitating the clinical introduction of new therapeutic strategies and their assessment.

Therefore, the aim of this work was to design and characterize a heat delivery system for ultrasound hyperthermia able to generate a uniform power deposition pattern in the target region with a closed-loop computational control, which would maintain temperature at a defined level indefinitely. A secondary aim of the work was to design a phantom test device on which to test and validate such systems. Similar systems have been reported using magnetic resonance (MR) thermometry [7]; however, the system presented herein uses thermocouples to monitor the temperature, offering the advantage of making it cheap and transportable. A review of focused ultrasound-based hyperthermia systems has been published elsewhere [8], in which thermocouples, MR thermometry, and infrared cameras have all been reported to measure temperature evaluation. There are a number of reviews of temperature monitoring techniques published [9], [10], detailing the advantages and disadvantages of each technique. Some systems are only applicable when the full body is heated to a constant temperature [11]. The ability to monitor temperature increases throughout thermal procedures is a regulatory prerequisite to clinical use in the USA alongside requirements to demonstrate the accurate targeting of a region of interest [12]. The spatial and temporal resolution required for such temperature measurements will depend on the specific application, including exposure time, rate of temperature rise, how the measurement it to be used (e.g., for feedback control versus dose calculation), and the delivery system used [9]. The development of an adaptable system for temperature control and monitoring is therefore of interest.

The hyperthermia delivery system presented herein is a flexible design with the ability to strictly control the induced temperature rise with a feedback loop. The system has the advantage that it can be reproduced elsewhere with relative ease and is adaptable for other temperature elevation applications, such as ablation therapy and for various tumor sizes/locations. The system was designed with an high intensity focused ultrasound (HIFU) transducer, coupled with a stand-off cone, which was characterized using National Physical Laboratory's (NPL) transducer characterization facility. The stand-off cone was a custom-made plastic cone, which was filled with deionized water and sealed with a Mylar layer. It ensures that the treatment is applied on a superficial surface at a specific distance from the transducer and provides a water path for coupling. The presented system has been designed for noninvasive treatment to superficial sites of interest; however, combined with simulations and without the use of the stand-off cone, the system could be expanded for nonsuperficial treatments. The use of a focused device and cones of different length allows for modification to extend the target region.

An application specific phantom device was designed to test the system performance. Ten exposures were performed, and the temperature achieved recorded over the heating phase for 4 min and the cooling phase for 4 min. Using both thermocouples and thermochromic tissue mimicking material (TMM) the temperature achieved, stability, repeatability, and localization of the treatment were assessed.

The designed system could be used for assessing the potential of radiotherapy combined with hyperthermia in initial phantoms and preclinical small animal studies.

II. SYSTEM REQUIREMENTS

The requirements of the system were as follows.

1) The transducer was required to have the ability to deliver up to 6 W over an alterable exposure region. An HIFU transducer was used to achieve this with a custom designed stand-off cone filled with degassed, deionized water, which could be replaced with others of different dimensions depending on the required region of exposure.

2) The aim of the system was to deliver an exposure, which generated a stable increase in temperature over a defined period. The acoustic power delivered by the ultrasound transducer therefore needed to be continuously adjusted to maintain a stable temperature at the focus. This required control of both the acoustic power delivered by the transducer and the ability to read and assess the current temperature at the focus throughout the exposure. This was achieved by fine control of the output acoustic power from the transducer throughout exposure, which was controlled through a feedback loop based on the temperature read at that moment. The acoustic power generated by the transducer is a function of the excitation voltage, and therefore, the ability to adjust this voltage throughout exposure was required. Thus, the system required software control of the excitation voltage, the ability to read and record the temperature in the exposed region throughout the exposure, and the ability to adjust the excitation voltage continuously based on this value.

3) The system was designed to be tested on a phantom device with biologically relevant acoustic and thermal properties, in which the exposure could be measured. The phantom device required the inclusion of some method of assessing the temperature increase in a feedback loop both at the center of the exposure region, to maintain the required temperature, and across the surface, to examine the heating profile to assess localization of treatment. A phantom test device was designed using a standard TMM, fine wire thermocouples, and thermochromic TMMs to fulfill this requirement.

III. SYSTEM DESIGN AND CHARACTERIZATION

A. Hyperthermia Delivery System

The ultrasound transducer used for this work was HIFU device (SU103 S/N 101, Sonic Concepts, Bothell, WA, USA). The center frequency of the transducer was 3.57 MHz.
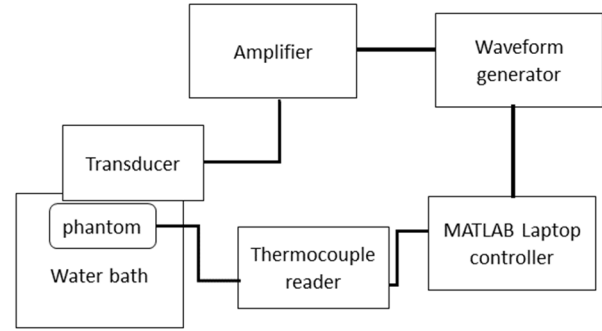

Fig. 1. Schematic of the experimental hyperthermia delivery system. The MATLAB (MATLAB 2019a, The Mathworks) controller adjusted the voltage on the waveform generator using a USB to general purpose interface bus (GPIB) interface.

A stand-off cone was attached and filled with degassed deionized water (conductivity <5 μS·cm^{-1}) and sealed with a 12-μm-thick Mylar layer (see Fig. 3). The characterization of the transducer is described in Section III-C. The transducer was powered by a system comprising a waveform generator (33250A, Agilent, Santa Clara, CA, USA) and amplifier (150A 100B, AR Ltd., Limerick, Ireland). The system was setup, as shown in Fig. 1. Prior to the system being switched ON, a specifically designed phantom, described in Section III-B, was submerged in a water bath, and the stand-off cone at the face of the transducer was positioned in contact with the in house manufactured thermochromic layer forming the top surface. The water bath was heated to 37 °C and the system switched ON.

The voltage delivered to the system was controlled via closed-loop feedback to the function generator with the drive voltage ranging between 30 and 55 mVpp (corresponding to 28.6–47.7 Vpp delivered to the transducer). The initial voltage was set to 30 mVpp. A thermocouple data logger (Pico universal serial bus (USB) TC 08, PicoTechnology, U.K.) read the temperature of the five thermocouples in the phantom via a MATLAB interface (R2019a, MATLAB, The Mathworks, MA, USA). The target temperature was set within the MATLAB code: the target here was set to body temperature, 37 °C, plus 6 °C:43 °C, and the upper and lower limits around this temperature set as T_{high} and T_{low}, respectively. When the temperature was read across the five thermocouples, the highest thermocouple temperature was compared to these values, if the temperature was lower than T_{low}, the voltage to the transducer was increased by 5 mVpp, and if the temperature was above T_{high}, the voltage to the transducer was decreased by 5 mVpp. The temperature was queried every 5 s for 4 min to first achieve heating in the target region and then maintain the temperature within this range. Thermocouple voltages and temperatures were recorded at each time point. After 4 min, the transducer was switched OFF, and the phantom began to cool, and the temperature was similarly queried and recorded every 5 s for 4 min in this period to determine the cooling curve. The experiment was repeated ten times with the phantom's single-use thermochromic TMM layer replaced each time. The limits of acceptable temperature were set to $T_{high} = 43.5$ °C and $T_{low} = 42$ °C in exposures 1–7 and further restricted to 43.5 °C and 42.5 °C in exposures 8–10.
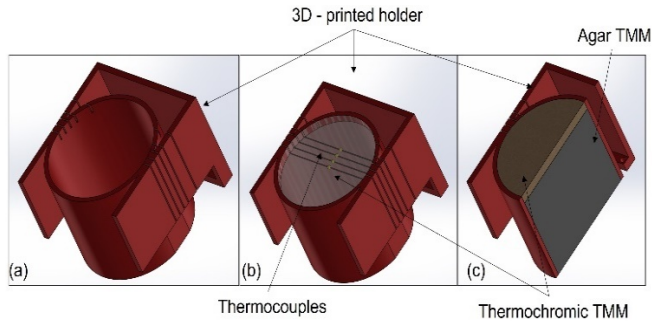
Fig. 2. Designed phantom test device. (a) 3-D printed holder, (b) with transparency of the thermochromic layer to show thermocouple positions, and (c) cross section showing the TMM layers. The overall phantom assembly was 35 mm in depth and 44 mm in diameter, the agar TMM section had a height of 32 mm, and the thermochromic layer 3 mm, both had a diameter of 38 mm.

B. Phantom Design

The phantom was designed with the following criteria: to simulate biological tissue acoustically and thermally, to provide real-time feedback of the temperature, and to include a thermochromic material to provide both an indicator of exposure area and the temperature reached in a biologically relevant environment. The phantom was designed containing fine wire thermocouples across the surface (see Fig. 2) held in place in a 3-D printed holder. There were 5 K-type 75-μm-diameter thermocouples (5SRTC-TT-KI-40-1M, Omega, U.K.) placed across the phantom: 1) at the center; 2) at 2.5 mm from the center; 3) at 5 mm; 4) at 7.5 mm; and 5) at the reference point (12.5 mm). The main body of the phantom was made of agar-based TMM and a layer of thermochromic TMM was placed on top (see Fig. 2). The main body of the phantom could therefore be reused, while the thermochromic layer was single use. The acoustic properties, as measured in NPLs characterization facility [13] and the thermal properties measured using a Tempos thermal property analyser (SH-3 probe, Meter Group, WA, USA) with a manufacturer stated uncertainty of 10%, of the TMMs used are detailed in Table I. The agar TMM was manufactured according to Annex DD.2 of International Electrotechnical Commission (IEC) standard 60601-2-37 [14]. The thermochromic material is based on a polyvinyl-alcohol cryogel (PVAc), and its manufacture is described in [15] with the addition of aluminum oxide scatterers. The thermal response of the ink used in the material manufactured for this study was sensitive between 42 °C and 43 °C (MB50Y-NH, Kromagen[1] Ink and Concentrates, Lawrence Industries, Tamworth, U.K.).

C. Transducer Characterization

The HIFU transducer was focused (diameter 23 mm and radius of curvature 35 mm) and a stand-off cone (height 49.50 mm) was attached to the face (see Fig. 3). The cone could be replaced with others of different dimensions designed for specific exposure areas. The adjusted transducer was characterized in terms of field mapping, acoustic pressure output,

[1]Traditional trademark.

TABLE I
ACOUSTIC AND THERMAL PROPERTIES OF THE TMM MEASURED IN THE DESIGNED PHANTOM

TMM type	Phase Velocity @ 3.5 MHz (m·s^{-1})	Attenuation @ 3.5 MHz (dB·cm^{-1})
Agar	1544 ± 5	2.2 ± 0.5
Thermochromic PVAc	1548 ± 5	2.1 ± 0.5

TMM type	Diffusivity (mm^2·s^{-1})	Volumetric specific heat (MJ·m^{-3}·K^{-1})	Conductivity (W·m^{-1}·K^{-1})
Agar	0.156	3.86	0.603
Thermochromic PVAc	0.160	3.77	0.603

Fig. 3. INRIM transducer comprising an SU103 S/N 101, Sonic Concepts transducer with stand-off cone, which was filled with deionized, degassed water, and fitted with a Mylar acoustic window for measurements.
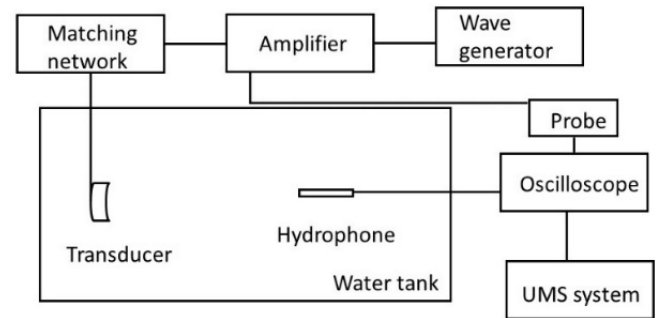

Fig. 4. Block diagram of the NPL scanning tank used for field mapping of the HIFU transducer.

and acoustic power output using NPL's calibration scanning tank and secondary standard power calibration service.

1) Field Mapping: The field map was obtained by mounting the transducer in the scanning tank (see Fig. 4) and using a calibrated (1–20 MHz and step-size 50 kHz) capsule hydrophone (Golden Lipstick, HGL-0200, Onda Corporation, Sunnyvale, CA, USA) to receive the signal generated at various positions relative to the transducer. The hydrophone had a 0.2 mm element diameter and was connected to a preamplifier (AG-2020) and dc block (AH-2020-DCBSW). The hydrophone was placed at a point within the far field of the ultrasonic trans-
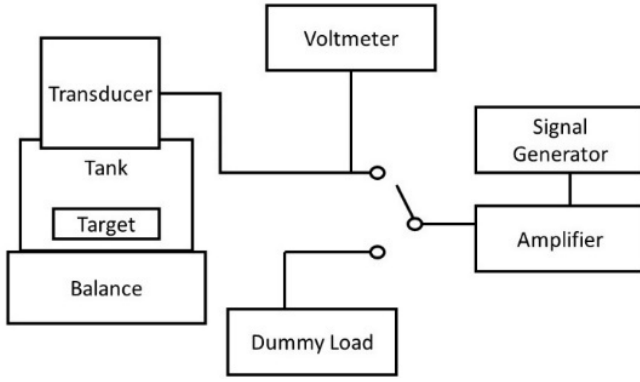
Fig. 5. Block diagram of the NPL secondary standard radiation force balance.

ducer radiating into a tank containing deionized water. The transducer was driven using a waveform generator (33250A, Agilent) and a power amplifier (150A100B, AR Ltd., Ireland). All measurement equipment was switched ON for a period of at least 1 h before measurements to ensure it reached thermal equilibrium. The transducer was excited by a 50-cycle sinusoidal tone-burst at 25.3 Vpp at the center frequency of the transducer (3.57 MHz). The hydrophone waveform was acquired following positioning and alignment for maximum signal in the plane perpendicular to the transducer axis [16]. The waveform received by the hydrophone was recorded using an oscilloscope (MS054, Tektronix, Beaverton, OR, USA). First, measurements were performed in planes perpendicular to the beam axis (XY planes), and a 2-D scan in the XY plane was performed with the hydrophone raster scanned across an area of 15 cm^2 around the focus in steps of 0.13 mm. Field mapping was performed both with and without the stand-off cone in place. Then, without the cone in place, a scan was performed from the far field to the near field region (-45 to $+15$ mm) in the XZ plane. Data were acquired using an ultrasound measurement system (UMS3, Precision Acoustics, U.K.), and waveforms were then passed through the postprocessing engine to output the peak positive voltage; then, using the previously calibrated hydrophone sensitivity, this was converted to peak positive pressure and the field map calculated. The measurements were made at 19.4 °C $\pm$ 0.5 °C.

The measured data from the XZ scan were read into MATLAB (MATLAB 2019a, The Mathworks), and assuming an axisymmetric field, an approximation of the XY plane was made by rotating the XZ scan around the axis at each axial distance, allowing for an estimation of the field at the cone face during exposures to be made.

2) Acoustic Output Power Calibration: The output power from the transducer was measured on the NPL secondary standard radiation force balance (RFB) based on absorbing target design (see Fig. 5) [17]. The power was measured at 21.4 °C $\pm$ 0.5 °C. The transducer was excited using continuous wave signals across the voltage range 20–56 Vpp and the power was measured at each voltage. The transducer was mounted at the top of the balance tank with its front face immersed in deionized, degassed water and radiating

vertically downward, and the centers of the transducer and the absorbing target (HAM A target, Precision Acoustics) were aligned along a vertical axis to within ±2 mm. The balance was interfaced with a PC, and the change in weight of the target was recorded as a function of time for the duration of each measurement set. In addition to the measurement of acoustic output power, the voltage supplied to the transducer was monitored. The RF voltage was measured at the end of the transducer cable using a high impedance (100 MΩ) probe connected to an oscilloscope (HDO4024A, Teledyne LeCroy, Teledyne Ltd., Thousand Oaks, CA, USA). For each delivered power, a measurement set consisted of four ON–OFF cycles, in which the voltage was delivered to the transducer during an ON cycle and a 50-Ω dummy load during the OFF cycle. The ON period was 7 s and the OFF period 20 s. The output was measured at two propagation distances of 5 and 4 mm from the target to the front face of the transducer and the transducer removed between measurements to provide a true repeat.

The measured power was calculated from the change in the measured mass at each ON–OFF–ON transition. The measured acoustic power P_m for an absorbing target is linearly related to the mean measured mass difference m by the following formula:

$$P_m = c \cdot m \cdot g \tag{2}$$

where c is the temperature-dependent speed of ultrasound in water and g is the gravitational acceleration (9.812 ms^{-2}). The radiated power P_r was then calculated using

$$P_r = \frac{P_m}{e^{-\alpha f^2 d} + k\left(1 - e^{-\alpha f^2 d}\right)} \tag{3}$$

where

f frequency of the ultrasonic wave (Hz);
d propagation distance (m);
k streaming constant for the target;
α intensity attenuation coefficient (s$^2 \cdot$m^{-1}).

D. Red, Green, and Blue (RGB) Image Analysis

Seven sample tubes of the thermochromic TMM were prepared. In turn, these were placed in a water bath and heated to defined temperatures up to 60 °C. By performing RGB analysis, the curves of color intensity versus temperature could then be established. After exposure, photographs were taken of the thermochromic TMM layers from the phantom and RGB analysis was performed of the region at the focus and a region at the exterior of the layer. The values were compared to the curves generated by RGB analysis of the sample tubes to assess the localization of the heating.

E. Repeatability

The repeatability of the system was approximated by calculating the thermal dose, CEM43, for each of the ten exposures performed. The thermal dose was calculated using (1) and inserting the temperature values at the central thermocouple for each exposure over the 8-min recording period, encompassing the heating and cooling curves recorded, to calculate the total dose.
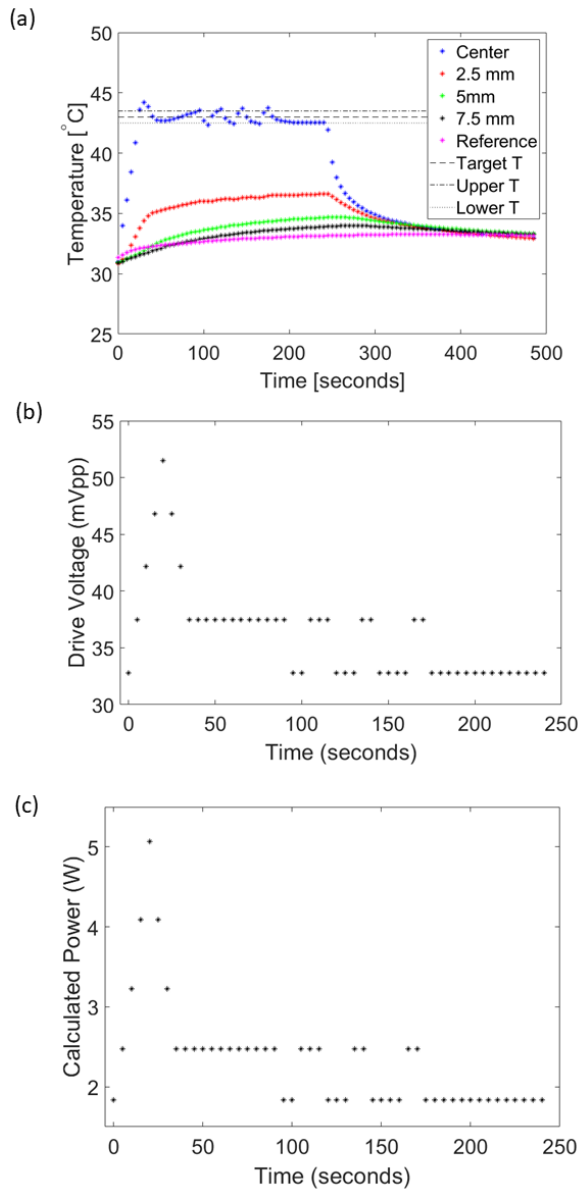
Fig. 6. Example of the recorded thermocouple temperatures and applied voltages from the phantom exposures, from run 10. (a) Temperature versus time, where the upper limit on temperature was 43.5 °C and the lower limit 42.5 °C. (b) Drive voltage versus time in the exposure phase. (c) Calculated power versus time in the exposure phase.

IV. RESULTS

A. Hyperthermia Delivery System

The hyperthermia delivery system was found to provide control of exposure based on the set temperature limits throughout all ten exposures. An example of the results is shown in Fig. 6.

The heating was also found to be sufficiently confined to the central focal region, with little effect on the thermocouple at 2.5 mm from the center and any perceivable change in the exterior thermocouples likely due to heat dissipation or heating due to the water bath temperature rise. The drive voltage and calculated power, based on the calibration curve from the NPL secondary standard, are also shown in Fig. 6; after an initial
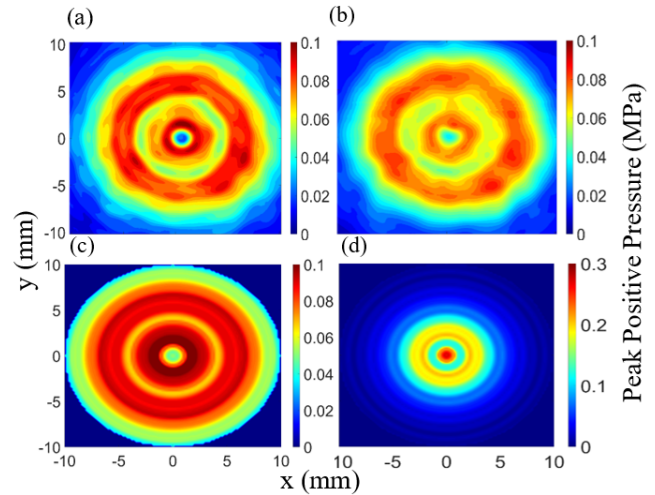

Fig. 7. XY plane field map (a) without the stand-off cone and (b) with the stand-off cone measured at 30 mm in the far-field and approximated fields at (c) 30 mm, for comparison, and (d) 15 mm after the focus, where exposures were performed.

rise during the heating phase, once the temperature stabilized, a relatively constant exposure was maintained, this might be further restricted using different upper and lower temperature limits and/or a smaller step-size in voltage increase. Once the transducer was switched OFF, the temperature rapidly decreased, confirming that the localized temperature-rise was induced by the exposure.

B. Transducer Characterization

The transducer output was measured on the NPL scanning tank. The field with and without the stand-off cone were compared. The cone was found to preserve the pressure levels and not distort the field of the transducer, with an average difference of 4%. Measurements at 30 mm in the far field are illustrated in Fig. 7(a) and (b). Assuming an axisymmetric field and using an XZ scan, the XY field at 30 mm was approximated [see Fig. 7(c)] and compared to the measured values. The agreement was found to be satisfactory, with less than 7% difference. The field at 15 mm after the focus was then approximated from the XZ scan [see Fig. 7(d)], which corresponds to the exposure distance due to the presence of the stand-off cone. The measurements, made during the exposure with both the thermocouples and the thermochromic TMM, qualitatively showed good agreement with the field map pattern. All results supported a strictly localized region of exposure, where only the central region would reach set target temperature.

The radiated power was measured on the NPL secondary standard RFB as a function of the recorded drive voltage, the results of which are shown in Fig. 8. The data fit to a power law of $P = 7.2 \times 10^{-3} \text{ Vpp}^{2.25}$ with a goodness-of-fit R^2 value of 1.

C. RGB Analysis of the Thermochromic TMM

After exposure RGB analysis was carried out on the samples of the thermochromic TMM, the thermochromic layers from
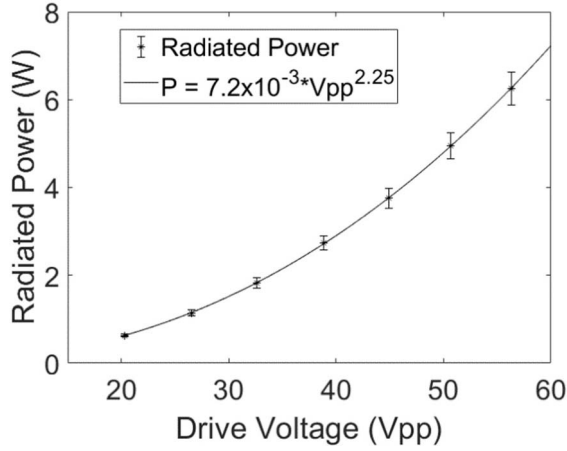
Fig. 8. Radiated power measured on the NPL secondary standard RFB as a function of the recorded drive voltage. The data fit to a power law of $P = 7.2 \times 10^{-3} \, Vpp^{2.25}$ with an R^2 of 1.

the phantom after exposure were compared to samples heated in a water bath to various fixed temperatures, and Fig. 9 illustrates these results. TMM samples in tubes were heated in a water bath to various temperatures between 25 °C and 60 °C [see Fig. 9(a)]. The color intensity of these samples was then extracted using RGB analysis and RGB curves with respect to temperature established [see Fig. 9(b)]. The most pronounced change in intensity was observed in the green curve across the color change threshold, in the range of the sensitivity of the ink (42 °C–43 °C).

Each of the single-use thermochromic TMM layers after exposure showed a confined area of darker lesion, where the exposure occurred, and no other lesions were present [see Fig. 9(c)]. This area matched the field maps for this position (−15 mm) (see Fig. 10). Areas in the exposure region and outside the exposure region were selected and RGB analysis indicated that the temperature achieved was at the target temperature in the exposure region and that the region exterior to this remained at body temperature. For example [see Fig. 9(d)], in the area selected exterior to the lesion $G = 143$, which corresponded to the temperature achieved in the water bath of 35 °C–37 °C, whereas for the area of the lesion itself $G = 119$, which corresponded to the target temperature on the RGB curve, 40 °C–43 °C. This analysis indicated that the system achieved sufficiently localized hyperthermia treatment and would not increase the temperature of the nontarget area above acceptable limits, which otherwise might lead to damage to healthy tissue.
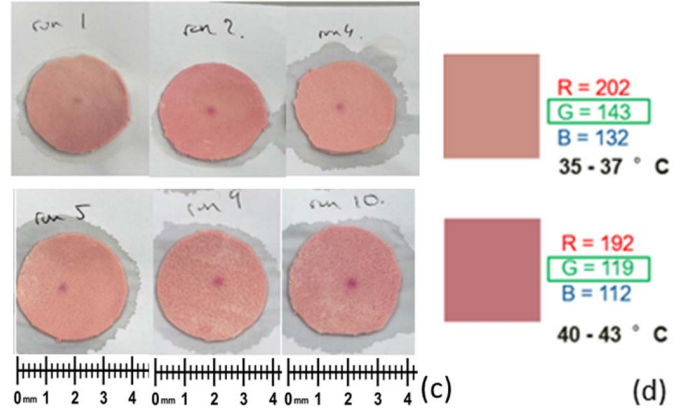
D. Repeatability

The thermal dose was calculated using (1) across all the exposures. The lower bound was found to have no significant effect on the delivered thermal dose when moving from 42 °C to 42.5 °C between exposures 1–7 and 8–10. The average thermal dose was found to be 2.36 ± 0.04 CEM at 43 °C, thus having a Type A uncertainty of less than 2% in the CEM43.
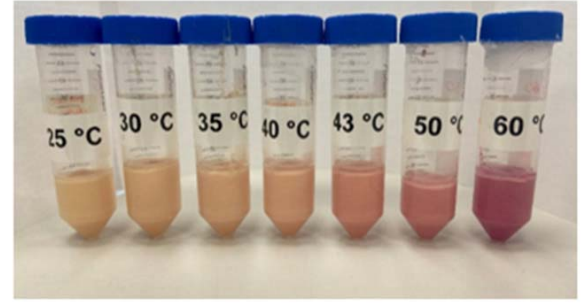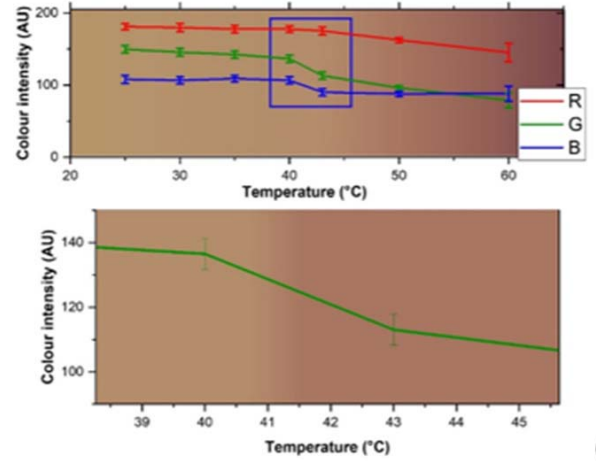
Fig. 9. RGB analysis of the thermochromic TMM. (a) TMM samples heated in a water bath to various temperatures, (b) RGB curves extracted from these samples overlaid on the color of the thermochromic TMM at each temperature, with a pronounced change in the green curve at the color change threshold, (c) various examples of the thermochromic TMM layers after exposure, showing a confined area of darker lesion, and (d) examples of the analysis on areas in the exposure region and outside the exposure region, indicating that the temperature achieved was at the target temperature and that the region exterior to this remained at body temperature.

V. LIMITATIONS OF THE STUDY

The developed system had the following limitations. The thermocouples are placed at discrete positions, therefore only giving an approximation of the heating across the surface at these specific points. While the thermochromic material
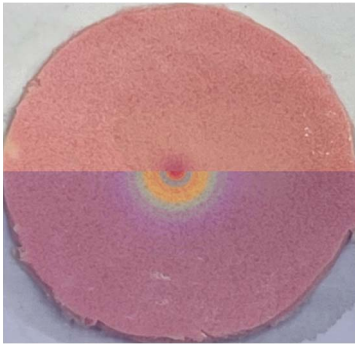
Fig. 10. Overlay of the semi-transparent half-field map at 15 mm, where the exposures were performed on a sample of the thermochromic TMM, showing that the region of exposure was well matched.

in some ways addresses this, there is also the potential that viscous heating and diffusion might be confounding the results in both measurement techniques. The use of smaller diameter thermocouples is recommended, where possible, to reduce the occurrence of such affects [18], [19]. Additionally, due to the small size of the thermocouples, there is some uncertainty in regard to the alignment of the phantom and the transducer, although due to the well localized heating, as evidenced on the thermochromic material, the presence of the exterior thermocouples in the phantom can be used to indicate whether the positioning is accurate within the discrete confines of the design. The thermochromic material indicated the exposure area in line with that expected; however, the change is irreversible and therefore gives no indication of stability of the temperature achieved across the exposure or of the cooling phase, only the maximum temperature. Additionally, the thermochromic layer was therefore not reusable and required replacement between exposures. Using the thermocouples and the thermochromic material combined addressed these limitations, somewhat, and was sufficient to ensure that the temperature did not rise above the prescribed maximum allowed, that the heating was sufficiently localized and could be maintained over a specified period, and that the thermal cooling could be accounted for when assessing the thermal dose.

VI. DISCUSSION AND SUMMARY

A bench-level hyperthermia delivery system was fully characterized and tested. The developed system successfully demonstrated the ability to induce a temperature rise in a tissue mimicking phantom and maintain that temperature indefinitely through a feedback loop. The use of a superficial thermocouple presents several advantages when compared to existing temperature monitoring systems. While the thermocouple only measures the superficial temperature, by avoiding implantation, the risk of hemorrhage is reduced [20]. The proposed solution is portable, cheap, and easy to implement. It does not require expensive equipment, such as a small animal MR machine capable of thermometry, and it is suitable for delivery of localized hyperthermia. The main drawback is the finite measurement of the temperature; however, an upgrade to an array of thermocouples would be straightforward. As with

all thermocouple-based measurements under continuous fields, viscous heating artifacts may affect the measurements; however, such measurements have been demonstrated to be more repeatable than MR thermometry [19].

The phantom designed allowed for assessment of temperature increase and localization of the treatment, through a combination of both; thermocouple readings at specific points, providing accurate feedback of the temperature throughout the exposure and cooling phases, and a thermochromic TMM, providing verification of the exposure localization. The results of this work contribute toward increasing confidence in the delivery of hyperthermia treatment to superficial tumors.

A clear advantage of the work presented herein is the fully characterized nature of the system combined with the unique phantom device, encompassing both thermocouples and thermochromic material to monitor exposure and its distribution, both throughout and after the treatment, thus providing a high level of confidence in the application of the treatment itself. The frequency of the transducer used in this system makes it suitable for superficial sites; however, the transducer may need to be substituted for lower frequencies for sites at greater depths [8].The system allowed control of the exposure based on temperature measured within adjustable limits, increasing or decreasing the delivered voltage to the transducer depending on the measured voltage compared to these limits. For all exposures present here, the target temperature was 43 °C, which is generally accepted to be the target for hyperthermia treatment and was in the sensitive range for the thermochromic ink, which was used in the thermochromic layer of the phantom. This target temperature could be adjusted for different applications if required and a different ink used in the thermochromic material, for example, that used in [15], where the material was sensitive from 52.5 °C.

Occasionally, the temperature increased above or decreased below the limitations set in the code when read by the thermocouples; at this point, the system would adjust the voltage to realign the exposure to deliver the required power. Any deviation from the target temperature could be further refined in three ways: 1) by reducing the range of acceptable temperatures; 2) by increasing the frequency of the temperature readings; and 3) by decreasing the voltage step applied when adjustments are implemented to the exposure. An initial buffer of, for example, 30 s in which the voltage is not adjusted, can also prevent any initial overshoot of the target temperature. Such adjustments to the parameters of the exposure could be made depending on the requirements of the exposure in question. The above disadvantages might be overcome through the use of proportional–integral–derivative (PID)-based temperature control, which has been used in the literature for hyperthermia systems before [21], potentially achieving a finer control. The data presented here demonstrated sufficient control for the requirements of this work.

The system was developed with the view to be fully characterized and validated at bench level. The work presented here demonstrated this through characterization of the transducer

and measurements with a phantom test object specifically designed for this purpose. The phantom design could be implemented for testing other such systems or the ink used in the thermochromic material could be substituted depending on the target temperature for thermal therapy systems designed for other applications. The hyperthermia delivery system was designed with small animal use in mind. The system was validated on a newly designed phantom. Future work will include implementing the system in a small animal study with the view to contributing to radiotherapy coupled with hyperthermia studies.

References

[1] P. B. Elming et al., "Hyperthermia: The optimal treatment to overcome radiation resistant hypoxia," *Cancers*, vol. 11, no. 1, p. 60, Jan. 2019, doi: 10.3390/cancers11010060.

[2] P. B. Dunscombe et al., (1989). *Report no. 027—Hyperthermia Treatment Planning*. [Online]. Available: https://doi.org/10.37206/26

[3] L. Zhu et al., "Ultrasound hyperthermia technology for radiosensitization," *Ultrasound Med. Biol.*, vol. 45, no. 5, pp. 1025–1043, May 2019, doi: 10.1016/j.ultrasmedbio.2018.12.007.

[4] H. P. Kok et al., "Heating technology for malignant tumors: A review," *Int. J. Hyperthermia*, vol. 37, no. 1, pp. 711–741, Jan. 2020, doi: 10.1080/02656736.2020.1779357.

[5] G. C. van Rhoon, T. Samaras, P. S. Yarmolenko, M. W. Dewhirst, E. Neufeld, and N. Kuster, "CEM43°C thermal dose thresholds: A potential guide for magnetic resonance radiofrequency exposure levels?" *Eur. Radiol.*, vol. 23, no. 8, pp. 2215–2227, Aug. 2013, doi: 10.1007/s00330-013-2825-y.

[6] G. C. van Rhoon, "Is CEM43 still a relevant thermal dose parameter for hyperthermia treatment monitoring?" *Int. J. Hyperthermia*, vol. 32, no. 1, pp. 50–62, Jan. 2016, doi: 10.3109/02656736.2015.1114153.

[7] M. E. Poorman et al., "Open-source, small-animal magnetic resonance-guided focused ultrasound system," *J. Therapeutic Ultrasound*, vol. 4, no. 1, p. 22, Dec. 2016, doi: 10.1186/s40349-016-0066-7.

[8] M. I. Priester, S. Curto, G. C. van Rhoon, and T. L. M. ten Hagen, "External basic hyperthermia devices for preclinical studies in small animals," *Cancers*, vol. 13, no. 18, p. 4628, Sep. 2021, doi: 10.3390/cancers13184628.

[9] I. Rivens, A. Shaw, J. Civale, and H. Morris, "Treatment monitoring and thermometry for therapeutic focused ultrasound," *Int. J. Hyperthermia*, vol. 23, no. 2, pp. 121–139, Jan. 2007, doi: 10.1080/02656730701207842.

[10] F. De Tommasi, C. Massaroni, R. F. Grasso, M. Carassiti, and E. Schena, "Temperature monitoring in hyperthermia treatments of bone tumors: State-of-the-art and future challenges," *Sensors*, vol. 21, no. 16, p. 5470, Aug. 2021, doi: 10.3390/s21165470.

[11] M. Salimi, S. Sarkar, M. Hashemi, and R. Saber, "Treatment of breast cancer-bearing BALB/c mice with magnetic hyperthermia using dendrimer functionalized iron-oxide nanoparticles," *Nanomaterials*, vol. 10, no. 11, p. 2310, Nov. 2020, doi: 10.3390/nano10112310.

[12] G. R. Harris, "FDA regulation of clinical high intensity focused ultrasound (HIFU) devices," in *Proc. Annu. Int. Conf. IEEE Eng. Med. Biol. Soc.*, Sep. 2009, pp. 145–148, doi: 10.1109/IEMBS.2009.5332444.

[13] S. Rajagopal, N. Sadhoo, and B. Zeqiri, "Reference characterisation of sound speed and attenuation of the IEC agar-based tissue-mimicking material up to a frequency of 60 MHz," *Ultrasound Med. Biol.*, vol. 41, no. 1, pp. 317–333, Jan. 2015, doi: 10.1016/j.ultrasmedbio.2014.04.018.

[14] *Particular Requirements for the Basic Safety and Essential Performance of Ultrasonic Medical Diagnostic and Monitoring Equipment*, document IEC 60601-2-37:2007, 2007.

[15] S. Ambrogio et al., "A polyvinyl alcohol-based thermochromic material for ultrasound therapy phantoms," *Ultrasound Med. Biol.*, vol. 46, no. 11, pp. 3135–3144, Nov. 2020, doi: 10.1016/j.ultrasmedbio.2020.07.032.

[16] *IEC 62127-1 ED 2, Ultrasonics–Hydrophones—Part 1: Measurement and Characterization of Medical Ultrasonic Fields*, Int. Electrotechnical Commision, Geneva, Switzerland, 2022. [Online]. Available: https://webstore.iec.ch/publication/6488

[17] *Radiation Force Balances and Performance Requirements (IEC 61161)*, Int. Electrotechnical Commision, Geneva, Switzerland, 2013. [Online]. Available: https://webstore.iec.ch/publication/4708

[18] W. J. Fry and R. B. Fry, "Determination of absolute sound levels and acoustic absorption coefficients by thermocouple probes—Theory," *J. Acoust. Soc. Amer.*, vol. 26, no. 3, pp. 294–310, May 1954, doi: 10.1121/1.1907332.

[19] S. Ambrogio et al., "A standard test phantom for the performance assessment of magnetic resonance guided high intensity focused ultrasound (MRgHIFU) thermal therapy devices," *Int. J. Hyperthermia*, vol. 39, no. 1, pp. 57–68, Dec. 2022, doi: 10.1080/02656736.2021.2017023.

[20] J. van der Zee, J. N. Peer-Valstar, P. J. Rietveld, L. de Graaf-Strukowska, and G. C. van Rhoon, "Practical limitations of interstitial thermometry during deep hyperthermia," *Int. J. Radiat. Oncol. Biol. Phys.*, vol. 40, no. 5, pp. 1205–1212, Mar. 1998, doi: 10.1016/s0360-3016(98)00008-x.

[21] A. Shikano, L. Tonthat, and S. Yabukami, "A simple and high-accuracy PID-based temperature control system for magnetic hyperthermia using fiber optic thermometer," *IEEJ Trans. Electr. Electron. Eng.*, vol. 16, no. 5, pp. 807–809, May 2021, doi: 10.1002/TEE.23361.

Aoife M. Ivory (Member, IEEE) received the B.A.(Mod) degree in physics with astrophysics, the M.Sc. degree in physical sciences in medicine, and the Ph.D. degree in ultrasound physics from Trinity College Dublin, Dublin, Ireland, in 2013, 2014, and 2018, respectively, focusing on the characterization of the ultrasound contrast agents and development of subharmonic imaging techniques for a clinical ultrasound system using novel phantom devices.

She is currently a Senior Research Scientist with the Ultrasound and Underwater Acoustics Group, National Physical Laboratory, Teddington, U.K. Her research focuses on photoacoustic imaging, ultrasonic characterization, and the development of tissue mimicking materials (TMMs) and phantoms.

Raphaela de Melo Baesso received the B.Sc. degree in industrial chemistry, the M.Sc. degree in chemical engineering, and the B.Sc. degree in chemical engineering from Federal Fluminense University, Niterói, Brazil, in 2011, 2013, and 2016, respectively, and the Ph.D. degree in biotechnology from the National Institute of Metrology, Quality and Technology (Inmetro), Duque de Caxias, Brazil, in 2018, focusing on biofuels production and quality control using low-power ultrasound.

She is currently the Quality Lead and a Higher Research Scientist with the Ultrasound and Underwater Acoustics Group, National Physical Laboratory, London, U.K. Her current interests are the development of the primary standard hydrophone calibration technique, materials characterization, therapeutic ultrasound, and quality assurance.

Giovanni Durando received the B.S. degree in physics from the University of Turin, Turin, Italy, in 1999, and the Doctorate degree in metrology from the Politecnico of Torino, Turin, in 2003.

In May 2009, he accepted a permanent position as a Physicist with the Advanced Materials Metrology and Life Science Department, Istituto Nazionale di Ricerca Metrologica (INRIM), Turin. His experimental activity is focused on acoustics, ultrasound, and metrology.

Dr. Durando is an Active Member of International Electrotechnical Commission-Technical Committee (IEC-TC) 87 (Ultrasonics) and is a Delegate for the Consultative Committee for Acoustic, Ultrasound and Vibration (CCAUV).

Srinath Rajagopal (Member, IEEE) received the B.Eng. degree in biomedical engineering from Visvesvaraya Technological University, Belgaum, India, in 2002, the M.Res. degree in biomedical engineering from the University of Strathclyde, Glasgow, U.K., in 2004, and the Ph.D. degree in the field of photoacoustics from the University College London, London, U.K., in 2019.

He was a Research Physicist with Precision Acoustics Ltd., Dorchester, U.K. Since joining NPL, Teddington, U.K., in 2007, he has been actively involved in the development of the ultrasound metrology infrastructure. He has built diagnostic and therapeutic ultrasound power primary standards and a secondary hydrophone calibration standard for National Measurement Institutes in Europe and Asia. He is currently the Science Area Leader of the Ultrasonics and Underwater Acoustics Group, NPL. He has authored at least 24 peer reviewed publications. He represents the U.K. on the International Electrotechnical Commission TC87/WG8 Ultrasonics—Field Measurements.

Piero Miloro received the M.Sc. degree in aerospace engineering from the University of Pisa, Pisa, Italy, in 2010, and the Ph.D. degree in biorobotics from Scuola Superiore Sant'Anna in Pisa, Pisa, in 2014.

He joined the Ultrasound and Underwater Acoustics Group, National Physical Laboratory, London, U.K., in 2015. He is currently a Senior Delivery Manager with the National Physical Laboratory. He has authored more than 30 peer reviewed articles. His current research interests are hydrophone calibration, materials characterization, therapeutic ultrasound, and safety of diagnostic ultrasound. He manages the medical ultrasound calibration services, which include hydrophone calibration, power measurements, and field and acoustic properties characterization.

Dr. Miloro is a member of the British Medical Ultrasound Society and the International Society of Ultrasound in Obstetrics and Gynecology, for which he is involved in the safety committees.